Research Article Vol. 6, No. 6 / June 2019 / Optica 823

Amplitude-multiplexed readout of single photon detectors based on superconducting nanowires

Alessandro Gaggero,[1,†,*] Francesco Martini,[1,2,†] Francesco Mattioli,[1] Fabio Chiarello,[1] Robert Cernansky,[2] Alberto Politi,[2] and Roberto Leoni[1]

[1]Istituto di Fotonica e Nanotecnologie—CNR, Via Cineto Romano 42, 00156 Roma, Italy
[2]Department of Physics and Astronomy, University of Southampton, Southampton SO17 1BJ, UK
*Corresponding author: alessandro.gaggero@ifn.cnr.it

Received 21 December 2018; revised 14 May 2019; accepted 15 May 2019 (Doc. ID 356104); published 20 June 2019

The realization of large-scale photonic circuits for quantum optics experiments at telecom wavelengths requires an increasing number of integrated detectors. Superconducting nanowire single photon detectors (SNSPDs) can be easily integrated onchip, and they can efficiently detect the light propagating inside waveguides. The thermal budget of cryostats poses a limit on the maximum number of elements that can be integrated on the same chip due to the thermal impact of the readout electronics. In this paper, we propose and implement a novel amplitude-multiplexing scheme allowing the efficient reading of several SNSPDs with only one readout port, thus enabling the realization of photonic circuits with a large number of modes.

https://doi.org/10.1364/OPTICA.6.000823

1. INTRODUCTION

Single photons are promising candidates as quantum bits (qubits) for quantum information applications due to their low decoherence and ease of transmission, both in free space and by means of optical fibers. Small- and medium-scale quantum computing [1] and simulation [2] can be realized by combining single-photon sources, single photon detectors, and linear optics. In the past 10 years, much effort has been devoted to developing an integrated platform containing all functionalities needed to achieve the tantalizing "quantum supremacy." Several experiments have been performed or proposed that exploit photonic integrated circuits (PICs), including boson sampling, quantum walk, and quantum simulation [3–7]. The complexity of the experiments reflects directly in the PIC architectures, requiring an always-increasing number of integrated components. All of the aforementioned experiments have been performed with hybrid setups, i.e., external sources and detectors, and a clear path to achieving a complete integrated platform is still lacking. SNSPDs are the only detectors [8] that showed on-chip integration feasibility with outstanding performance in terms of detection efficiency, dark count rate, and timing resolution in the infrared wavelength range [9–16]. The PIC architecture requires the integration of several tens of SNSPDs, posing new challenges related to the simultaneous readout of different channels. The use of dedicated readout electronics for each detector channel is not a practical solution and has a tremendous impact on the thermal budget allowed by cryostats. To overcome these limitations, several multiplexing schemes have been proposed based on different approaches. A row–column multiplexing scheme enables the readout of planar 2D array of N^2 detectors with only 2N channels [17]. Another proposal is based on frequency multiplexing and uses different RF resonators to read out an SNSPD array, where the switching of a portion of the nanowire causes a shift in the resonator operating frequency. Although with this technique it is possible to read out a huge number of detectors, each RF tone needs a demultiplexing circuit, thus limiting the maximum filling factor achievable by the array [18]. Time domain approaches have been also exploited, where, by using a time-tagged multiplexing scheme, the signals coming from two SNSPDs were separated in time using a delay line [19]. This approach requires only a single readout line, but has no photon number resolution, and the overall dimensions of the array are dictated by the design of the delay line. Another time tagging scheme was employed to demonstrate a single photon imager using a continuous nanowire delay line. This device was able to resolve the position of absorbed single photons [20]. More recently, another implementation based on time multiplexing was reported [21], where the authors show a two-terminal detector based on a superconducting nanowire microstrip transmission line. The transmission line works as an array that can resolve the position of more than one photon and naturally acts as a coincidence counter. However, to resolve the position of two photons simultaneously, the reference time that generates the double firing event is needed. In addition, a maximum photon number resolution of up to four photons was demonstrated using a complex post processing of the array voltage pulse.

In this work, we implemented a novel and simple scheme that is able to read out multiple SNSPDs with only one coaxial cable without the requirement of complex postprocessing. The scheme presented here has similarities with previous realizations of photon number resolving architectures (PNR) [22–24] but expands such

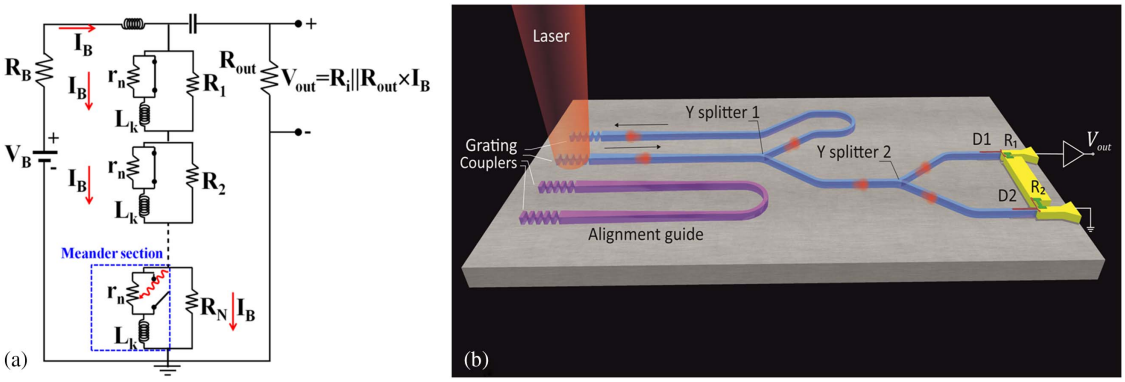

Fig. 1. (a) Sketch of the electrical scheme used to read the pulsed signal at the output of an N-element array. Each element of the array is made by a SNSPD (represented in the sketch with a switch, the normal resistance r_n, and the wire kinetic inductance L_k) with an on-chip AuPd resistance R_i in parallel (see text). A bias-tee is used to bias and read out the array. (b) Integrated experiment scheme, consisting of an array of two SNSPDs and a PIC made of two 50:50 Y splitters and input/output ports.

prior art for relevant multiplexing applications, thanks to the capability to discriminate the position where the photon is absorbed. This property is of paramount importance in quantum integrated photonics. The readout scheme [see Fig. 1(a)] is based on the amplitude multiplexing of N active elements consisting of a SNSPD in parallel with an on-chip AuPd resistor, R_i. When a photon is absorbed in an active element, a normal resistance r_n appears in the superconductive nanowires [25,26] and, being $r_n \gg R_i$ by design (typically $r_n \sim 1$ kΩ), all the bias current is diverted to the parallel resistance R_i. The position of the photon-absorption event is then encoded in the voltage amplitude of the pulse, $V_{\text{out}} = R_i \| R_{\text{out}} I_B$. Because of the compact readout scheme, we were able to show a proof of concept based on a two-element array integrated in a silicon nitride (Si_3N_4) PIC [see Fig. 1(b)]. In addition, to retrieve the specific properties of each SNSPD, the circuit is intrinsically able to implement $g^{(2)}(\tau)$ measurements [27,28]. Combining our approach with the use of a cryogenic amplifier, tens of detectors can be read with a single coaxial cable with a minimum thermal impact on the operating temperature.

2. FABRICATION

To show the resolution capability of our approach, we design the parallel resistances R_1 and R_2 as $R_2 = 2 \cdot R_1$. The detectors D_1 and D_2 [Figs. 2(b) and 2(c)], connected in series, are integrated on the PIC [Fig. 2(a)] and the nanowire length is chosen to be 30 μm, ensuring good photon absorption up to 77% in the NbN nanowires at wavelength 1550 nm. The thickness of the Si_3N_4 layer (350 nm) and the width (1.9 μm) of the waveguides are chosen to minimize the optical losses (expected to be 5 dB/cm) while maintaining the absorption in the nanowires as high as possible.

The device fabrication exploits four steps of electron beam lithography (EBL). The first step is used to define the integrated PIC on the Si_3N_4 layer that is deposited by PECVD on a 2 μm thick thermal SiO_2 [29]. The waveguide pattern [Fig. 2(a)] is written on a 400 nm thick CSAR resist and is then transferred to the Si_3N_4 using an inductively coupled plasma (ICP) reactive ion etching (RIE). Successively, a 6 nm thick NbN film is sputtered on the PIC by DC magnetron sputtering at $T = 550$°C in a gas mixture of $N_2 + \text{Ar}$ (with 22% N_2). Using a second step of EBL, we define the Ti/Au electric contacts on PMMA via lift-off (10/60 nm thick, respectively). The NbN nanowires (80 nm wide) are then patterned on 180 nm thick HSQ resist used as an etching mask for the removal of the unwanted NbN [see Figs. 2(b) and 2(c)]. Finally, the AuPd resistances are fabricated via lift-off of a Ti (5 nm)/AuPd (85 nm) film.

3. ELECTRO-OPTICAL CHARACTERIZATION

To avoid the use of expensive and bulky cryogenic positioners, we align and glue a Pyrex fiber array (FA), composed of

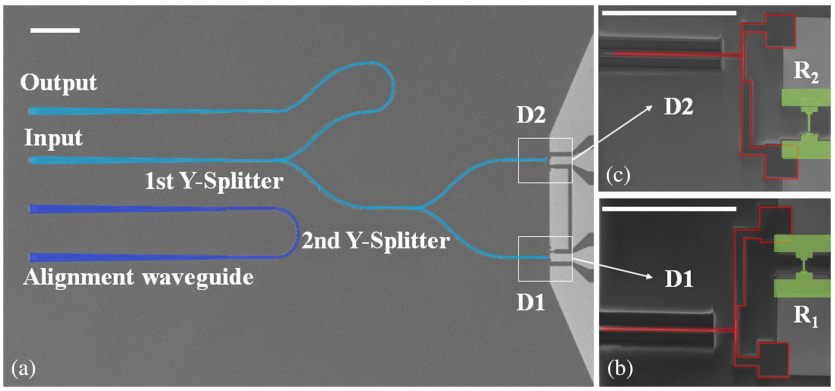

Fig. 2. (a) Scanning electron micrograph of the SNSPD array consisting of two detectors (D_1 and D_2) integrated on top of a PIC made of two 50:50 Y splitters and input/output ports realized with grating couplers; the scale bar corresponds to 125 μm. Enlarged views of (b) D_1 and (c) D_2. The scale bars are 30 μm. In green are highlighted the parallel resistance R_1 and R_2, respectively.

6 single-mode fibers, to the ports of the PIC, obtaining in this way fast and reliable light coupling. The alignment is obtained at room temperature by maximizing the light at the control port of the photonic circuit [see Fig. 2(a)] thanks to a six-axis manipulator for the FA. The coupling efficiency of the grating coupler is about 15% at room temperature. Successively, the chip is mounted on a GM refrigerator operating at a temperature $T = 2.9$ K. During the sample cooling, the transmitted optical power decreases due to the different thermal contractions between the Pyrex (FA) and the silicon substrate, causing a reduction of the coupling efficiency down to ∼2%. The readout electronics implements a chain of two bias-tees and two RF amplifiers with a gain of 49 dB in the bandwidth 0.1–500 MHz.

A. Pulse Position Resolution

The NbN 80 nm wide and 6 nm thick nanowire has a 9 K critical temperature and a critical current density of 3.9 MA/cm^2 at 2.9 K. The travelling photons at 1550 nm wavelength, generated by a 10 ps pulsed laser, are injected through the input port of the PIC. Figure 3(a) shows a single shot trace of the array acquired with a 4 GHz bandwidth oscilloscope and a laser repetition rate of 10 MHz. Three different pulse amplitudes, related to the values of R_1, R_2, and $R_1 + R_2$, are observed due to the firing events of D_1 and D_2. The higher pulse is due to the simultaneous firing of D_1 and D_2, attesting to a coincidence event. Using an exponential fit for the pulses, it is possible to evaluate the recovery time of the two peaks related to R_1 and R_2, corresponding respectively to $\tau_1 = 11.81$ ns and $\tau_2 = 6.10$ ns. The recovery times are in agreement with a decay time proportional to the inverse of the resistance ($\tau_i = L_k/R_i$ [30], with the nanowire kinetic inductance L_k equal for both detectors). Figure 3(b) displays the persistence map of the array output signal, showing the three amplitude levels, taken with a bias current of 17 μA.

For this measurement, we chose to work with an average photon number $\langle\mu\rangle = 1$ to increase the probability of a coincidence event that otherwise would be very low in the single photon regime. By using this plot, it is possible to reconstruct the histogram of the amplitude probabilities [see Fig. 3(c)] considering a temporal slice taken at 700 ps [green line of Fig. 3(b)]. Using a Gaussian fit we retrieve the position of the three maxima, corresponding to $V_1 = (-31.8 \pm 9.6)$ mV, $V_2 = (-53.7 \pm 9.4)$ mV, and $V_3 = (-84.6 \pm 9.8)$ mV. From the peak voltage positions and considering $I_B = 17$ μA, we found $R_1 = 7.81\Omega$ and $R_2 = 14.98\Omega$, in good agreement with the expected values of R_1 and $R_2 \approx 2 \cdot R_1$.

B. Array Efficiency

The inset of Fig. 4(a) shows the on-chip detection efficiency (ODE) and dark count rate (DCR) of the array as a function of the bias current, measured under the illumination of a pulsed laser with $\lambda = 1550$ nm, pulse width of 10 ps, and a repetition rate $f = 1$ MHz, while the DCR was measured with the laser off. The power of the laser was attenuated down to an average photon per pulse $\langle\mu\rangle = 0.1$ corresponding to the single photon regime. The array has a maximum ODE of about 24% at a DCR of ∼3 kHz and an ODE 11% at 10 Hz of DCR [inset of Fig. 4(a)]. The effect of the different pulse amplitudes generated by D_1 and D_2 is clearly illustrated when recording the pulse count rate as a function of the voltage trigger level of the frequency counter from −100 to −10 mV [see Fig. 4(a)]. We can clearly individuate three levels in the count rate. The first plateau level (in the range from −10 to −30 mV) includes the counts due to D_1 (pulses with the lowest amplitude), D_2, and those due to the coincidences coming from the simultaneous firing of both D_1 and D_2. The second plateau (in the range from −35 to −55 mV) takes into account pulses coming from D_2 and from the simultaneous firing of the two detectors, while the third plateau (in the range from −65 to −90 mV) is due only to the coincidence events. The plot in Fig. 4(a) is obtained by subtracting the dark count events to the counts for each bias current. In the range from −10 to 0 mV, the counts due to the firing of D_1 and D_2 are dominated by the contribution of the electronic noise that is eliminated with the subtraction of the dark counts.

Considering that 10^5 photons/s are coupled at the input of the second 50:50 Y splitter, from Fig. 4(a) we can extrapolate the relative ODEs of D_1 and D_2 that correspond to 30.4% and 15.6%, respectively [see Fig. 4(b)]. These efficiencies are underestimated, as no losses are taken into account due to the last part of the photonic circuit (from the second Y splitter to the detectors).

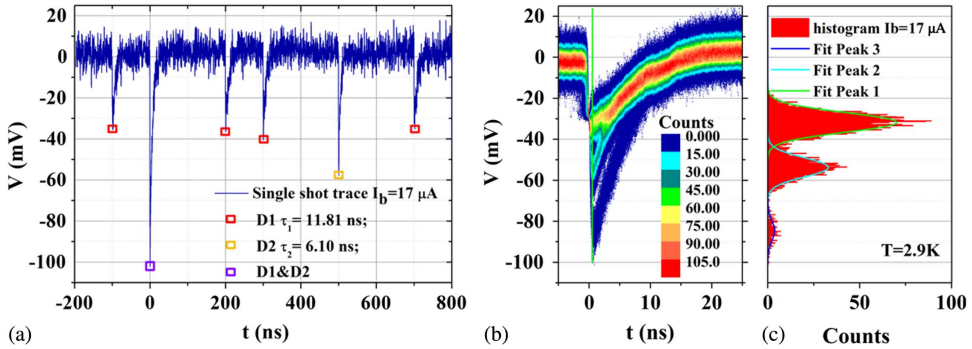

Fig. 3. (a) Single trace of the array output signal showing peaks with three different heights due to the firing of D_1 (with R_1 in parallel, red squares), D_2 (with R_2 in parallel, yellow squares), and the simultaneous firing of D_1 and D_2 (purple squares) at $I_B = 17$ μA. The exponential fit of the decay time provides a value of $\tau_1 = 11.81$ ns and $\tau_2 = 6.10$ ns for the peaks due to D_1 and D_2, respectively. (b) Persistence map of the transient response of the array under the illumination of a 10 ps pulsed laser with 10 MHz repetition rate and an average photon number per pulse $\langle\mu\rangle = 1$. (c) Histogram of pulse counts as a function of voltage, obtained from the persistence plot using data of the slice taken at 700 ps [green vertical line in (b)] and its fits with three Gaussian curves (continuous lines).

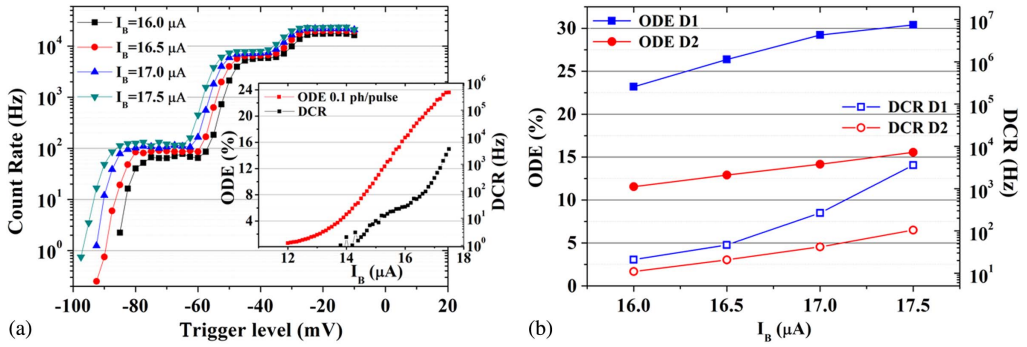

Fig. 4. (a) Pulse count rate of the array versus trigger voltage level of the counter measured at different bias currents for 10^5 photons/s photon flux coupled to the input of the second Y splitter. Inset: ODE of the array (red squares) and DCR (black squares) as a function of the bias current, taken at $T = 2.9$ K. (b) ODE and DCR of individual D_1 and D_2, respectively.

4. SCALABILITY

The scalability of our approach depends on three main parameters: the input resistance of the readout electronics R_{out} (generally coincides with the RF amplifier impedance), the maximum resistance value R_M allowed by the system, and the signal-to-noise ratio (SNR). In our setup, R_M is limited by the 50 Ω input resistance of the RF amplifier being R_{out} in parallel with the SNSPD array [see Fig. 1(a)]. This poses a limit to the maximum pulse amplitude $V_{\max} = I_B \cdot R_M$. In the single photon regime, only one detector is firing at once, implying that the rules required for the selection of the set of resistances are $R_i \neq R_{i+1}$ and $\Delta R = R_{i+1} - R_i$ large enough to produce voltage signals greater than the amplifier noise. Therefore, the maximum number of channels readable with a single coax cable is $Ch = R_M/\Delta R$. With $R_M = 50$ Ω, the scalability of our scheme can be increased by reducing ΔR as low as possible.

Table 1 summarizes three cases. The first row takes into account all the parameters we measured in our experiment, the second row describes how we can improve our scalability using a commercially available cryogenic RF amplifier [33], while the third one refers to an amplifier with an input impedance of 1 kΩ.

The fit of the three peaks of the histogram [Fig. 3(c)] provides a maximum variance $2\sigma = (7.4 \pm 0.1)$ mV corresponding to peak 2, giving a noise resistance $\Delta R_{2\sigma} \approx 1.6$ Ω (amplifier gain $G = 49$ dB), in close agreement with $\Delta R_{\text{th}} = 1.2$ Ω calculated from the Johnson–Nyquist voltage noise that is expected for an RF amplifier working at room temperature $T = 300$ K [31].

As shown in the second row of Table 1, a reduction of a factor 15 of the amplifier working temperature corresponds to an increase of SNR of a factor ∼4. The SNR can also be improved increasing the bias current I_B by improving the film quality, by tuning the geometric parameters of the nanowires, or by connecting several nanowires in parallel [34,35]. In the latter case, we expect an I_B increase of at least a factor 2.

By selecting an appropriate resolution determined by the step resistances, $\Delta R_{2\sigma}$ and $\Delta R_{6\sigma}$, we can identify the firing element of the array with 68.3% probability and 99.7%, respectively, where the choice strongly depends on the application. For example, if detectors would be used as pixels for spectroscopy or imaging, an uncertainty in the precise position of the firing detector might be tolerated. When error rates have to be minimized, like in quantum computation, it is possible to assign the values of R_i in a strategic way and make use of additional delay lines to separate in time pulses with close voltage amplitudes and thus reject erroneous events.

In the single photon regime and considering that the maximum pulse amplitude is $V_M = I_B \cdot R_M$, where $R_M = 50$ Ω, we can calculate the maximum number of elements that can be read, given by $\text{Ch}_{6\sigma} = 50/\Delta R_{6\sigma} = 10$ channels at 300 K and $\text{Ch}_{6\sigma} = 41$ at 20 K. If we consider a less stringent step resolution of $\Delta R_{2\sigma}$, the maximum number of channels rises to $\text{Ch}_{2\sigma} = 30$ at 300 K and $\text{Ch}_{2\sigma} = 121$ at 20 K. Estimating the number of channels Ch, we neglected the fit error because it provides a small uncertainty in the peak discrimination.

In the multiphoton regime, the firing of different channels occurs simultaneously, increasing the number N of Gaussian peaks to be discriminated. For example, the number N of levels required to resolve the position of two elements firing simultaneously is $N = \text{Ch}(\text{Ch} - 1)/2$ [36]. In the case of a 50 Ω RF amplifier at $T = 300$ K (first row of Table 1), the maximum number of channels that can be read in a two photon regime is $\text{Ch}_{2\sigma} \approx 8$, which becomes ∼16 by cooling the amplifier at 20 K. However, the lack of linearity due to the parallel with 50 Ω input impedance of the amplifier complicates the selection rules for the resistance steps. The linearity requirements in the

Table 1. Figures of Merit Regarding the Array Readout Scalability in Single Photon Regime[a]

R_{Out}(Ω)	T(K)	B(MHz)	I_B(μA)	ΔR_{th}(Ω) [31]	$\Delta R_{2\sigma}$(Ω)	$\Delta R_{6\sigma}$(Ω)	R_M(Ω)	$\text{Ch}_{6\sigma}$	$\text{Ch}_{2\sigma}$
50	300	0.1–500	17	1.20	1.60	4.70	50	10	30
50	20	0.1–500	17	0.31	0.41 [32]	1.20 [32]	50	41	121
1000	20	0.1–500	17	1.40	1.90 [32]	5.70 [32]	200	35	105

[a]For a selected RF amplifier, R_{out} is its input resistance, T the working temperature, and B the bandwidth. ΔR_{th} is the noise resistance due to thermal noise [31], while $\Delta R_{2\sigma}$ and $\Delta R_{6\sigma}$ are the resistance step values obtained considering 2σ and 6σ given by the width of the Gaussian fits. The R_M is the maximum resistance allowed by the system; $\text{Ch}_{6\sigma}$ and $\text{Ch}_{2\sigma}$ are the numbers of detectors for $\Delta R_{2\sigma}$ and $\Delta R_{6\sigma}$, respectively.

multiphoton regime can be met by implementing a high-impedance cryogenic readout (row 3 in Table 1). In this case, the conditions required for R_M are $R_M \ll R_{\text{out}}$, to preserve the linearity, and $R_M < R_{\text{lat}}$, to ensure the recovery of the nanowire superconductivity, with R_{lat} as the resistance value that causes the latching of the nanowires in a stable normal state [37]. The high input resistance of the amplifier increases ΔR_{th}, resulting in total numbers of levels of 105 and 35, which can be equally spaced by the values $\Delta R_{2\sigma}$ and $\Delta R_{6\sigma}$, respectively. In the multiphoton regime, when multiple elements switch simultaneously, the recovery time speed is shorter than $\tau_{\max} = L_k/\Delta R_{6\sigma}$, given by the firing of the element with the lowest $R_i = \Delta R_{6\sigma}$ [38]. This implies that the worst-case scenario is given by the single photon regime, where the detector with the smallest parallel resistance switches.

5. CONCLUSION

We demonstrated an easy-to-use and scalable architecture for the readout of multiple superconducting detectors integrated in a high-dimensional PIC. In the single photon regime, amplitude multiplexing holds an advantage over other approaches in terms of implementation complexity, compactness, and photon number resolution capability. In addition, the amplitude multiplexing readout is more convenient than the row–column scheme up to a number of detectors $N_{\text{SNSPD}} \leq 4\ \text{Ch}^2$ [39]. The amplitude multiplexing approach is compatible with amorphous superconducting materials [40] and other techniques used to overcome the low fabrication yield of SNSPDs [13,41]. Our proposal has a tremendous importance in the field of photonic quantum technologies, where experiments like boson sampling, quantum walk, and photonic quantum computing require the reading of a large number of modes. With the proposed approach, the positions of single photons propagating in more than 100 channels can be resolved with a single coax cable. This architecture allows the reduction of the thermal load inside cryostats, which is a key point toward the realization of large-scale integrated experiments using SNSPDs.

Funding. H2020 Future and Emerging Technologies (FET) (641039); H2020 Marie Skłodowska-Curie Actions (MSCA) (795923); Ministero dell'Istruzione, dell'Università e della Ricerca (MIUR) (543/2015).

†These authors contributed equally to this work.

REFERENCES AND NOTES

1. E. Knill, R. Laflamme, and G. J. Milburn, "A scheme for efficient quantum computation with linear optics," Nature **409**, 46–52 (2001).
2. A. Aspuru-Guzik and P. Walther, "Photonic quantum simulators," Nat. Phys. **8**, 285–291 (2012).
3. A. Politi, M. J. Cryan, J. G. Rarity, S. Yu, and J. L. O'Brien, "Silica-on-silicon waveguide quantum circuits," Science **320**, 646–649 (2008).
4. A. Peruzzo, M. Lobino, J. C. F. Matthews, N. Matsuda, A. Politi, K. Poulios, X. Zhou, Y. Lahini, N. Ismail, K. Wörhoff, Y. Bromberg, Y. Silberberg, M. G. Thompson, and J. L. O'Brien, "Quantum walks of correlated photons," Science **329**, 1500–1503 (2009).
5. N. Spagnolo, C. Vitelli, M. Bentivegna, D. J. Brod, A. Crespi, F. Flamini, S. Giacomini, G. Milani, R. Ramponi, P. Mataloni, R. Osellame, E. F. Galvão, and F. Sciarrino, "Experimental validation of photonic boson sampling," Nat. Photonics **8**, 615–620 (2014).
6. A. Crespi, R. Osellame, R. Ramponi, V. Giovannetti, R. Fazio, L. Sansoni, De. F. Nicola, F. Sciarrino, and P. Mataloni, "Anderson localization of entangled photons in an integrated quantum walk," Nat. Photonics **7**, 322–328 (2013).
7. J. Wang, S. Paesani, Y. Ding, R. Santagati, P. Skrzypczyk, A. Salavrakos, J. Tura, R. Augusiak, L. Mančinska, D. Bacco, D. Bonneau, W. J. Silverstone, Q. Gong, A. Acín, K. Rottwitt, L. K. Oxenløwe, J. L. O'Brien, A. Laing, and M. G. Thompson, "Multidimensional quantum entanglement with large-scale integrated optics," Science **360**, 285–291 (2015).
8. R. Hadfield, "Single-photon detectors for optical quantum information applications," Nat. Photonics **3**, 696–705 (2009).
9. J. P. Sprengers, A. Gaggero, D. Sahin, S. Jahanmirinejad, G. Frucci, F. Mattioli, R. Leoni, J. Beetz, M. Lermer, M. Kamp, S. Höfling, R. Sanjines, and A. Fiore, "Waveguide superconducting single-photon detectors for integrated quantum photonic circuits," Appl. Phys. Lett. **99**, 181110 (2011).
10. W. H. P. Pernice, C. Schuck, O. Minaeva, M. Li, G. Goltsman, A. V. Sergienko, and H. X. Tang, "High-speed and high-efficiency travelling wave single-photon detectors embedded in nanophotonic circuits," Nat. Commun. **3**, 1325 (2012).
11. C. Schuck, W. H. P. Pernice, and H. X. Tang, "Waveguide integrated low noise NbTiN nanowire single-photon detectors with milli-Hz dark count rate," Sci. Rep. **3**, 1893 (2013).
12. D. Sahin, A. Gaggero, Z. Zhou, S. Jahanmirinejad, F. Mattioli, R. Leoni, J. Beetz, M. Lermer, M. Kamp, S. Höfling, and A. Fiore, "Waveguide photon-number-resolving detectors for quantum photonic integrated circuits," Appl. Phys. Lett. **103**, 111116 (2013).
13. F. Najafi, J. Mower, N. C. Harris, F. Bellei, A. Dane, C. Lee, X. Hu, P. Kharel, F. Marsili, S. Assefa, K. K. Berggren, and D. Englund, "On-chip detection of non-classical light by scalable integration of single-photon detectors," Nat. Commun. **6**, 5873 (2013).
14. G. Reithmaier, M. Kaniber, F. Flassig, S. Lichtmannecker, K. Müller, A. Andrejew, J. Vuckovic, R. Gross, and J. J. Finley, "On-chip generation, routing, and detection of resonance fluorescence," Nano Lett. **15**, 5208–5213 (2015).
15. P. Rath, O. Kahl, S. Ferrari, F. Sproll, G. Lewes-Malandrakis, D. Brink, K. Ilin, M. Siegel, C. Nebel, and W. Pernice, "Superconducting single photon detectors integrated with diamond nanophotonic circuits," Light Sci. Appl. **4**, e338 (2015).
16. A. Vetter, S. Ferrari, P. Rath, R. Alaee, O. Kah, V. Kovalyuk, S. Diewald, G. N. Goltsman, A. Korneev, C. Rockstuh, and W. H. P. Pernice, "Cavity-enhanced and ultrafast superconducting single-photon detectors," Nano Lett. **16**, 7085–7092 (2016).
17. M. S. Allman, V. B. Verma, M. Stevens, T. Gerrits, R. D. Horansky, A. E. Lita, F. Marsili, A. Beyer, M. D. Shaw, D. Kumor, R. Mirin, and S. W. Nam, "A near-infrared 64-pixel superconducting nanowire single photon detector array with integrated multiplexed readout," Appl. Phys. Lett. **106**, 192601 (2015).
18. S. Doerner, A. Kuzmin, S. Wuensch, I. Charaev, F. Boes, T. Zwick, and M. Siegel, "Frequency-multiplexed bias and readout of a 16-pixel superconducting nanowire single-photon detector array," Appl. Phys. Lett. **111**, 032603 (2017).
19. M. Hofherr, M. Arndt, K. Il'in, D. Henrich, M. Siegel, J. Toussaint, T. May, and H. G. Meyer, "Time-tagged multiplexing of serially biased superconducting nanowire single-photon detectors," IEEE Trans. Appl. Supercond. **23**, 2501205 (2013).
20. Q. Y. Zhao, D. Zhu, N. Calandri, A. E. Dane, A. N. McCaughan, F. Bellei, H. Z. Wang, D. F. Santavicca, and K. K. Berggren, "Single-photon imager based on a superconducting nanowire delay line," Nat. Photonics **11**, 247–251 (2017).
21. D. Zhu, Q. Y. Zhao, H. Choi, T. J. Lu, A. E. Dane, D. Englund, and K. Berggren, "A scalable multi-photon coincidence detector based on superconducting nanowires," Nat. Nanotechnology **13**, 596–601 (2018).
22. A. Divochiy, F. Marsili, D. Bitauld, A. Gaggero, R. Leoni, F. Mattioli, A. Korneev, V. Seleznev, N. Kaurova, O. Minaeva, G. Gol'tsman, K. G. Lagoudakis, M. Benkhaoul, F. Lévy, and A. Fiore, "Superconducting nanowire photon-number-resolving detector at telecommunication wavelengths," Nat. Photonics **2**, 302–306 (2008).
23. S. Jahanmirinejad, G. Frucci, F. Mattioli, D. Sahin, A. Gaggero, R. Leoni, and A. Fiore, "Photon-number resolving detector based on a series array of superconducting nanowires," Appl. Phys. Lett. **101**, 072602 (2012).
24. F. Mattioli, Z. Zhou, A. Gaggero, R. Gaudio, R. Leoni, and A. Fiore, "Photon-counting and analog operation of a 24-pixel photon number

resolving detector based on superconducting nanowires," Opt. Express **24**, 9067 (2016).
25. J. J. Renema, G. Frucci, Z. Zhou, F. Mattioli, A. Gaggero, R. Leoni, M. J. A. de Dood, A. Fiore, and M. P. van Exter, "Universal response curve for nanowire superconducting single-photon detectors," Phys. Rev. B **87**, 174526 (2013).
26. J. J. Renema, R. Gaudio, Q. Wang, Z. Zhou, A. Gaggero, F. Mattioli, R. Leoni, D. Sahin, M. J. A. de Dood, A. Fiore, and M. P. van Exter, "Experimental test of theories of the detection mechanism in a nanowire superconducting single photon detector," Phys. Rev. Lett. **112**, 117604 (2014).
27. D. Sahin, A. Gaggero, T. B. Hoang, G. Frucci, F. Mattioli, R. Leoni, J. Beetz, M. Lermer, M. Kamp, S. Höfling, and A. Fiore, "Integrated autocorrelator based on superconducting nanowires," Opt. Express **21**, 11162 (2013).
28. M. Schwartz, E. Schmidt, U. Rengstl, F. Hornung, S. Hepp, S. L. Portalupi, K. Llin, M. Jetter, M. Siegel, and P. Michler, "Fully on-chip single-photon Hanbury-Brown and Twiss experiment on a monolithic semiconductor-superconductor platform," Nano Lett. **18**, 6892–6897 (2018).
29. R. Cernansky, F. Martini, and A. Politi, "Complementary metal-oxide semiconductor compatible source of single photons at near-visible wavelengths," Opt. Lett. **43**, 855 (2018).
30. A. J. Kerman, E. A. Dauler, W. E. Keicher, J. K. W. Yang, K. K. Berggren, G. Gol'tsman, and B. Voronov, "Kinetic-inductance-limited reset time of superconducting nanowire photon counters," Appl. Phys. Lett. **88**, 111116 (2006).
31. $R_{\mathrm{th}} = V_n/I_B$, with $v_n = (4\,k_{\mathrm{B}}\mathrm{TBR}_{\mathrm{out}})^{1/2}$ given by the Johnson noise of the amplifier resistance at $T = 300$ K and $I_B = 17$ μA.
32. This value have been derived from the ΔR_{th} considering at least a broadening similar to the case at 300 K.
33. http://www.caltechmicrowave.org/amplifiers.
34. M. Ejrnaes, R. Cristiano, O. Quaranta, S. Pagano, A. Gaggero, F. Mattioli, R. Leoni, B. Voronov, and G. Gol'tsman, "A cascade switching superconducting single photon detector," Appl. Phys. Lett. **91**, 262509 (2007).
35. F. Marsili, F. Najafi, E. Dauler, F. Bellei, X. Hu, M. Csete, R. J. Molnar, and K. K. Berggren, "Single-photon detectors based on ultranarrow superconducting nanowires," Nano Lett. **11**, 2048–2053 (2011).
36. In general, $\mathrm{N} = \sum_{\mathrm{n}=1}^{\mathrm{Ch}} \binom{\mathrm{Ch}}{n} = \mathrm{Ch} + \binom{\mathrm{Ch}}{2} + \binom{\mathrm{Ch}}{3} + \ldots = \mathrm{Ch} + \frac{\mathrm{Ch}(\mathrm{Ch}-1)}{2} + \frac{\mathrm{Ch}(\mathrm{Ch}-1)(\mathrm{Ch}-2)}{6} + \ldots = 2^{\mathrm{Ch}} - 1$ is the number of levels necessary to discriminate n photons. In Table 1 $N = Ch$, as we are discussing the case $n = 1$, i.e., the single photon regime.
37. L. Zhang, L. You, X. Yang, J. Wu, C. Lv, Q. Guo, W. Zhang, H. Li, W. Peng, Z. Wang, and X. Xie, "Hotspot relaxation time of NbN superconducting nanowire single-photon detectors on various substrates," Sci. Rep. **8**, 1486 (2018).
38. S. Jahanmirinejad and A. Fiore, "Proposal for a superconducting photon number resolving detector with large dynamic range," Opt. Express **20**, 5017–5028 (2012).
39. In the single photon regime (see Table 1), with amplitude multiplexing the number of coax lines N^{AM} required to encode N_{SNSPDs} detectors is $N^{\mathrm{AM}} = N_{\mathrm{SNSPD}}/\mathrm{Ch}$, while in the case of the row–column readout, the number of coax lines needed is $N^{\mathrm{RC}} = 2\sqrt{N_{\mathrm{SNSPD}}}$. The condition $N^{\mathrm{AM}} < N^{\mathrm{RC}}$ is satisfied for $N_{\mathrm{SNSPDs}} \leq 4\ \mathrm{Ch}^2$. For example, for $\mathrm{Ch}_{6\sigma} = 35$, amplitude multiplexing is still superior up to $N_{\mathrm{SNSPD}} = 4900$ because it uses fewer coax lines. The advantage is even more evident in the 2σ case, where the readable channel Ch is larger.
40. F. Marsili, V. B. Verma, J. A. Stern, S. Harrington, A. E. Lita, T. Gerrits, I. Vayshenker, B. Baek, M. D. Shaw, R. P. Mirin, and S. W. Nam, "Detecting single infrared photons with 93% system efficiency," Nat. Photonics **7**, 210–214 (2013).
41. R. Gourgues, I. E. Zadeh, A. W. Elshaari, G. Bulgarini, J. W. N. Los, J. Zichi, D. Dalacu, P. J. Poole, S. N. Dorenbos, and V. Zwiller, "Controlled integration of selected detectors and emitters in photonic integrated circuits," Opt. Express **27**, 3710–3716 (2019).